



CO₂ methanation over nickel-ZrO₂ catalyst supported on carbon nanotubes: A comparison between two impregnation strategies

M. Romero-Sáez^{a,b,*}, A.B. Dongil^c, N. Benito^d, R. Espinoza-González^a, N. Escalona^{e,f}, F. Gracia^{a,*}

^a Department of Chemical Engineering, Biotechnology and Materials, FCFM, Universidad de Chile, Beauchef 851, Santiago, Chile

^b Quality, Metrology and Production Group, Instituto Tecnológico Metropolitano, Campus Robledo, Calle 73 No. 76A - 354, Medellín, Colombia

^c Department of Physical Chemistry, Laboratory of Catalysis by Metals, Universidad de Concepción, Edmundo Larenas 129, Concepción, Chile

^d Department of Physics, Universidad de Concepción, Casilla 160-C, Concepción, Chile

^e Department of Chemical Engineering and Bioprocesses, Pontificia Universidad Católica de Chile, Avda. Vicuña Mackenna 4860, Macul, Santiago, Chile

^f Facultad de Químicas, Pontificia Universidad Católica de Chile, Chile



ARTICLE INFO

Keywords:

CO₂ methanation
Impregnation
Nickel catalysts
Zirconia
Carbon nanotubes

ABSTRACT

Ni-ZrO₂ catalysts supported on CNT synthesized by sequential and co-impregnation were tested in the CO₂ methanation reaction. The catalysts were characterized using different physico-chemical techniques including BET surface area analysis, TGA, H₂-TPR analysis, CO₂-TPD analysis, XRD analysis, TEM-EDS analysis and XPS. Both samples were found to be active in the CO₂ methanation; however, the catalyst prepared by co-impregnation was notably less active and selective to CH₄ than the catalyst synthesized by sequential impregnation method. The characterization results gave significant insight on the disposition of active phases in CNT surface. The catalyst prepared by co-impregnation showed NiO nanoparticles surrounded by ZrO₂ in core-shell structures that growth over the CNT, reducing reactant access to Ni and Ni – ZrO₂ interface. Additionally, TEM analysis of this catalyst prepared by sequential impregnation showed NiO nanoparticles available and deposited either on the surface or next to the ZrO₂ nanoparticles, increasing the extent of the Ni – ZrO₂ interface thus improving the catalytic performance.

1. Introduction

The decrease in the reserves of fossil fuels is one of the main problems in the current world, which force its efficient use and find alternatives energy sources. Also related to the use of fossil fuels, the increase in emissions of CO₂, which is one of the most abundant gases present in the Earth's atmosphere, is one of current environmental concerns, and this making necessary the use of this compound by different ways. Therefore, the development of appropriate strategies for the use of CO₂ could be an interesting alternative for the current energy and environmental problems.

Among the different processes for the use of CO₂ (capture, sequestration, conversion, etc.), the production of CH₄, which is an actual energy compound of wide use, through hydrogenation, has been an effective method for the consumption of CO₂ [1]. The CO₂ methanation reaction has been known for a long time, and it was first introduced by Sabatier and Senderens [2]. In last years, this reaction has been investigated using a number of catalytic systems based on VIIIB metals (e.g., Ru [3,4], Rh [5], Pd [6], and Ni [7–9]) supported on various oxides [3–9] (e.g., Al₂O₃, TiO₂, SiO₂, ZrO₂, and CeO₂). Among them,

the nickel-based catalysts have been extensively investigated under various conditions for their comparatively lower price and relatively higher activity.

Most of the catalysts are commonly prepared by impregnation, in which the oxide support is contacted with a solution of a salt or other soluble compound containing the desired metal. The different preparation methods have shown that the performance of the catalyst greatly depends on the synthesis methodology. Thus, the dispersion of the active phase, which will influence the accessibility of reagents, and the metal-support interaction, which often involves a synergistic effect important for a good catalytic performance, are strongly influenced by the method of preparation [10,11].

In recent years, carbon nanotubes have raised much interest due to their exceptional properties. As a new type of novel nano-carbon catalyst support, they have high surface area, unique electronic properties and chemical inertness, thermal stability, high mechanical strength and unique tubular structure [12–14]. These properties can efficiently improve the dispersion of the active components and enhance the adsorption of reactants. Therefore, using carbon nanotubes as support would be also interesting to optimize the use of active phases by

* Corresponding authors at: Department of Chemical Engineering, Biotechnology and Materials, FCFM, Universidad de Chile, Beauchef 851, Santiago, Chile.
E-mail addresses: manuel.romero@ing.uchile.cl (M. Romero-Sáez), fgracia@ing.uchile.cl (F. Gracia).

dispersing them onto a high surface area support. There are several works that have synthesized bimetallic or metal/oxide catalysts supported on carbon nanotubes, either by co-impregnation [15,16] or by sequential impregnation [17,18], confirming that the preparation strategy could condition the properties and the behavior of the catalyst.

For all of these reasons, in this work Ni-ZrO₂ catalyst supported on CNT were synthesized by both methods: sequential impregnation and co-impregnation, in order to elucidate difference in the interaction between Ni and ZrO₂ and to correlate these findings with the preparation method and catalytic performance during CO₂ Methanation. The catalysts were characterized by N₂ adsorption-desorption, XRD, TGA, CO₂-TPD, H₂-TPR, TEM-EDS and XPS techniques and correlated with the catalytic performance.

2. Methods

2.1. Catalysts preparation

Commercial multiwalled carbon nanotubes (CNT) Nanocyl 3100 (> 95% purity) were used as starting material. Ni/ZrO₂/CNT catalysts were prepared by sequential impregnation (SEQ) and co-impregnation (COI). Ni content (5 wt.%) was selected based on previous studies and literature, while ZrO₂ content was set at 20 wt.% based on preliminary dispersion studies in CNT, evaluating different concentrations of ZrO₂ (5, 10, 20 and 40 wt.%).

Ni/ZrO₂/CNT-SEQ: For the zirconium precursor impregnation, the corresponding amount of ZrO(NO₃)₂ xH₂O (99.99%, Sigma-Aldrich) was dissolved in acetone to achieve a 20% wt. loading. The CNT were added to the solution, in a proportion of 10 ml g⁻¹ of support with stirring. After 12 h in a covered flask, the excess of solvent was slowly removed in a rotary evaporator under vacuum, until complete removal of the solvent at room temperature during the whole process. The solid was dried for 24 h at 80 °C. Finally, the solid was heat treated during 5 h at 350 °C under flowing argon (50 ml min⁻¹), with a heating rate of 1 °C min⁻¹. After this process, the nickel was incorporated by using the proper amount of Ni(NO₃)₂ (99.9%, Sigma-Aldrich) dissolved in acetone to obtain 5 wt.% Ni, with 10 ml of solution per gram of solid. After stirring for 12 h, the solvent was removed under vacuum at 60 °C. Finally, the material was treated at 350 °C for 5 h under flowing Ar (50 ml min⁻¹).

Ni/Zr/CNT-COI: For the synthesis of this catalyst, the same zirconium and nickel precursors were dissolved in acetone along with the CNT loading employing the same amounts as those for the Ni/Zr/CNT-SEQ amounts. Then, the same procedure for impregnation in a rotatory evaporator, drying and heat treatment was applied.

Ni/CNT: For the sake of comparison, a 5 wt.% Ni catalyst was prepared over parent CNTs following the same experimental procedure.

2.2. Characterization techniques

The surface area of the prepared catalysts were determined by N₂ adsorption-desorption at -196 °C using a Micromeritics ASAP 2010 equipment. The BET method [19] was used to calculate the total surface area of the catalysts.

Temperature-programmed reduction (H₂-TPR) analysis was carried out in a quartz reactor, and the gases were detected by a thermal conductivity detector. The sample (0.10 g) was placed in the reactor and was subjected to the following analysis sequence. First, the catalyst was oxidized under a stream of pure O₂ (40 cm³ min⁻¹) with a temperature ramp of 10 °C min⁻¹ from room temperature to 300 °C. The temperature was maintained at 300 °C for 1 h, and then decreased to room temperature under the same stream of pure O₂. Finally, the sample was cleaned under a stream of pure Ar (40 cm³ min⁻¹) at room temperature. The reducing gas used in all experiments was 5%H₂/Ar, with a flow rate of 20 cm³ min⁻¹. The temperature range explored was from room temperature to 600 °C with a heating rate of 10 °C min⁻¹.

This temperature was maintained for 30 min so as to complete the reduction process. The water produced by reduction was trapped into a water trap.

CO₂ temperature-programmed desorption (CO₂-TPD) measurements were carried out on an OmniStar GSD 320 O1 (Pfeiffer Vacuum) mass spectrometer to monitor the desorption of CO₂. Prior to adsorption experiments, the samples (50 mg) was first reduced under a pure hydrogen stream (40 cm³ min⁻¹) at 500 °C. Then, they were cooled down to 50 °C in an Ar flow before the CO₂ adsorption started. The adsorption step was performed in 10%CO₂/He flow (40 cm³ min⁻¹) at 50 °C for 1 h. Subsequently, the sample was exposed to a flow of Ar (40 cm³ min⁻¹) for 1 h at 50 °C in order to remove reversibly and physically adsorbed CO₂ from the surface. Finally, desorption was carried out from 50 to 600 °C at a heating rate of 10 °C min⁻¹ in Ar stream (40 cm³ min⁻¹).

X-ray diffraction (XRD) analyses were carried out at room temperature in a Bruker D8 Advance diffractometer, using Cu K α irradiation at $\lambda = 1.54 \text{ \AA}$; the scanning angle range was 10-80° with an increment of 0.02° and time per step of 0.5 s. Just before the measurements, the samples were pretreated at 500 °C for 1 h in flowing pure H₂ (80 ml min⁻¹), cooling under He flow, and handled for the analysis.

Thermal stability of the samples was measured by thermogravimetric analysis (TGA), heating the catalysts from room temperature up to 900 °C at 10 °C min⁻¹ under synthetic air flow (20 cm³ min⁻¹) in a thermogravimetric analyzer (NETZSCH TG 209-F1 Libra).

X-ray photoelectron spectroscopy (XPS) spectra were obtained using a hemispherical analyser (Physical Electronics 1257 system). A twin anode (Mg and Al) X-ray source was operated at a constant power of 200 W using Al K α radiation (1486.6 eV) for the XPS measurements. Just before the measurements, the samples were pretreated at 500 °C for 1 h in flowing pure H₂ (80 ml min⁻¹), cooling under He flow, and handled for the analysis. Then, the sample was placed in a sample stage in which the emission angle can be varied. In this case, the emission angle was 45°.

Transmission electron microscopy (TEM) and Energy-dispersive X-ray spectroscopy (EDS) analysis were conducted in a FEI Tecnai F20 Transmission Electron Microscope operated at 200 kV. Just before the measurements, the samples were pretreated at 500 °C for 1 h in flowing pure H₂ (80 ml min⁻¹), cooling under He flow, and handled for the analysis. Then, they were dispersed in isopropanol by ultrasonic stirring for 15 min and the dispersion was dropped in carbon-copper grids. In order to remove organic contamination, the grids were exposed to an argon plasma cleaning before microscopy measurements.

2.3. Reaction conditions and experimental reaction set-up

CO₂ methanation experiments were carried out in a fixed-bed quartz reactor with an inner diameter of 9.4 mm, at atmospheric pressure and temperature range 200–500 °C. The thermocouple was directly inserted into the catalyst bed to measure the actual pretreatment and reaction temperatures. The reactor was loaded with 0.30 g of catalyst in each experiment. Prior to the reaction, the sample was reduced at 500 °C for 1 h in flowing pure H₂ (80 ml min⁻¹). After the catalyst reduction, the reactor was flushed with pure He and the temperature decreased to 200 °C. Then, the reactants are fed from original mixtures 10% CO₂ in He, and 10% H₂ in He. The flow of each mixture is controlled by mass flow controllers to set a reactant mixture CO₂:H₂:He entering the reactor with a molar ratio 1:5:94, total gas flow of 100 cm³ min⁻¹. These reaction conditions resulting in a GHSV value of 75.000 ml h⁻¹ g⁻¹. These experimental conditions have been proven to prevent any mass transfer limitation. An on-line gas chromatograph (Perkin Elmer Clarus 500) equipped with a Grace CTR-I packed column, and a Thermal Conductivity Detector (TCD) was used to quantify the concentration of gases in the reactor inlet and exit.

Table 1

Composition, BET surface areas and XPS data of prepared catalysts.

Sample	Ni, %	ZrO ₂ , %	CNT, %	S _{BET} , m ² g ⁻¹	Ni 2p _{3/2}			Zr 3d	
					Ni ⁰ , %	Ni–O, %	Ni ^{x+} , %	Zr–O, %	Zr ^{x+} , %
CNT	0	0	100	300	–	–	–	–	–
Ni/CNT	5	0	95	255	72	28	–	–	–
Ni/Zr/CNT-COI	5	20	75	209	48	19	33	60	40
Ni/Zr/CNT-SEQ	5	20	75	202	25	40	35	64	36

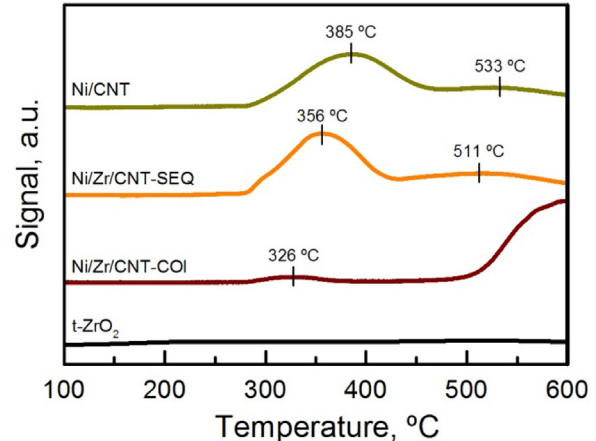
3. Results and discussion

3.1. Catalyst characterization

Specific surface areas of the catalyst are summarized in Table 1. BET surface area showed by pure CNT was 300 m² g⁻¹, and this value decreased when they were impregnated with Ni or Ni and Zr. Ni/Zr/CNT-COI and Ni/Zr/CNT-SEQ catalysts presented very similar BET surface areas of 209 and 202 m² g⁻¹, respectively. The decrease in S_{BET} can be mainly ascribed to the incorporation of two solid oxides with much lower surfaces areas, since this reduces the surface of the whole catalyst per mass of material. However, the incorporation of NiO and ZrO₂ crystallites in the free space among the bundles of the tubes, can be also responsible of the S_{BET} decrease. On the other hand, specific surface of Ni/CNT catalyst was 255 m² g⁻¹, value higher than those of the zirconia-containing catalysts, so there is clear effect due to the presence of Zr. Nonetheless, the effect of Ni is comparatively larger than that of Zr, as the initial CNT surface area is reduced in 17% for Ni/CNT with 5 wt % of NiO, whereas this reduction only doubles (30% for Ni/Zr/CNT-COI and 32% for Ni/Zr/CNT-SEQ) with the inclusion of 20 wt% of ZrO₂.

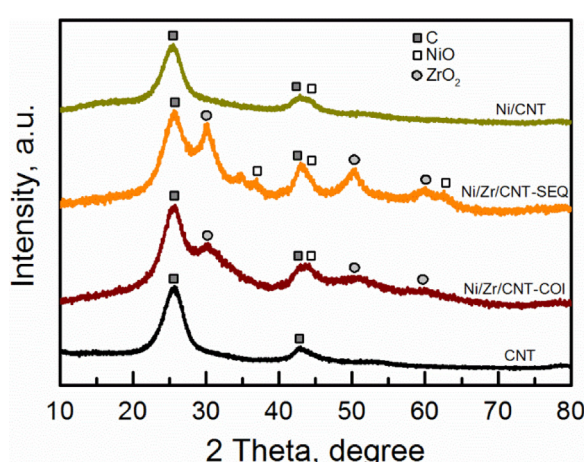
The results of thermogravimetric analysis in air of the samples (see supplementary material) indicated that the CNT and all the catalysts were thermally stable with no weight loss up to 500 °C, which was the highest temperature used in the methanation reactions.

Fig. 1 shows XRD patterns of the catalysts and the CNT used in this work. All samples showed strong diffraction peaks at 26.1° and 43.5°, which were assigned to the (002) and (101) reflections of the graphite in CNT, respectively [20,21]. The position and sharpness of the C (002) peak in the three catalysts diffractograms indicated that the graphite structure of the CNT was well preserved without significant damage after the oxides deposition. Ni/Zr/CNT-SEQ catalyst showed three low intensity reflections at 2θ = 37.0°, 43.8° and 62.1°, which can be indexed as (111), (200) and (220) crystal planes of the NiO, respectively [22,23]. These signals are observed much more clearly in this catalyst than in the other two samples containing Ni, where they are hardly seen. This suggested that the crystallinity of NiO in Ni/Zr/CNT-SEQ

Fig. 2. H₂-TPR profiles of the different catalyst.

catalyst was greater. Ni/Zr/CNT-SEQ and Ni/Zr/CNT-COI samples showed the three most intense signals of tetragonal ZrO₂ pattern at 2θ = 30.5°, 50.1° and 60.0°, which were assigned to the (101), (112) and (211) reflections, respectively [24,25]. As in previous cases, these signals were broader and smaller in Ni/Zr/CNT-COI catalyst, and this was attributed to poor crystallinity and/or to a smaller crystallite size of the tetragonal ZrO₂ powders in this catalyst [26].

The reducibility of the catalyst was investigated by H₂-TPR (Fig. 2). Ni/Zr/CNT-SEQ and Ni/CNT catalysts presented a very similar reduction profile. Both samples showed a first strong signal, which started around 300 °C, and a second weaker signal centered at 500–550 °C. The first signals, centered between 350 and 400 °C, were assigned to highly dispersed NiO interacting weakly with the support [27,28]. Whereas the high temperature peak from about 400 to 600 °C corresponded to highly dispersed nickel oxides in intimate contact with the exterior walls of the CNTs [15]. The similar shape and H₂ consumption of these two samples suggested that NiO nanoparticles in Ni/Zr/CNT-SEQ sample are easily accessible to H₂ in the catalyst surface. In addition, it can be seen that the presence of ZrO₂ effectively promoted the reduction of the nickel oxides. Comparing these two samples, the high reduction peak decreased from 385 °C for Ni/CNT to 356 °C for Ni/Zr/CNT-SEQ, and the weaker signal decreased from 533 to 511 °C. This suggested more easily reducible nickel species on the surface of Ni/Zr/CNT-SEQ catalyst, which may be ascribed to a different interaction between the metal oxides and the CNT support by the addition of zirconia. Similar results were reported for Ni-CeO₂-CNT systems [15,17]. On the other hand, Ni/Zr/CNT-COI sample showed a very different reduction profile. The intensity of the first signal was very low, indicating that a lower portion of Ni was available for reduction at low temperatures. In addition, the second reduction signal was very intense, and it appeared at higher temperatures compared to the other two catalysts. These results clearly indicate that, in the catalyst prepared by co-impregnation, nickel was not easily available for its reduction. Furthermore, H₂-TPR of ZrO₂ showed no reduction signal at all tested temperatures, suggesting that, in Ni/Zr/CNT-COI sample, Ni was mostly covered/blocked by zirconia after co-impregnation. Because of that, a higher

Fig. 1. XRD patterns of the NiO-ZrO₂-CNT catalysts and CNT.

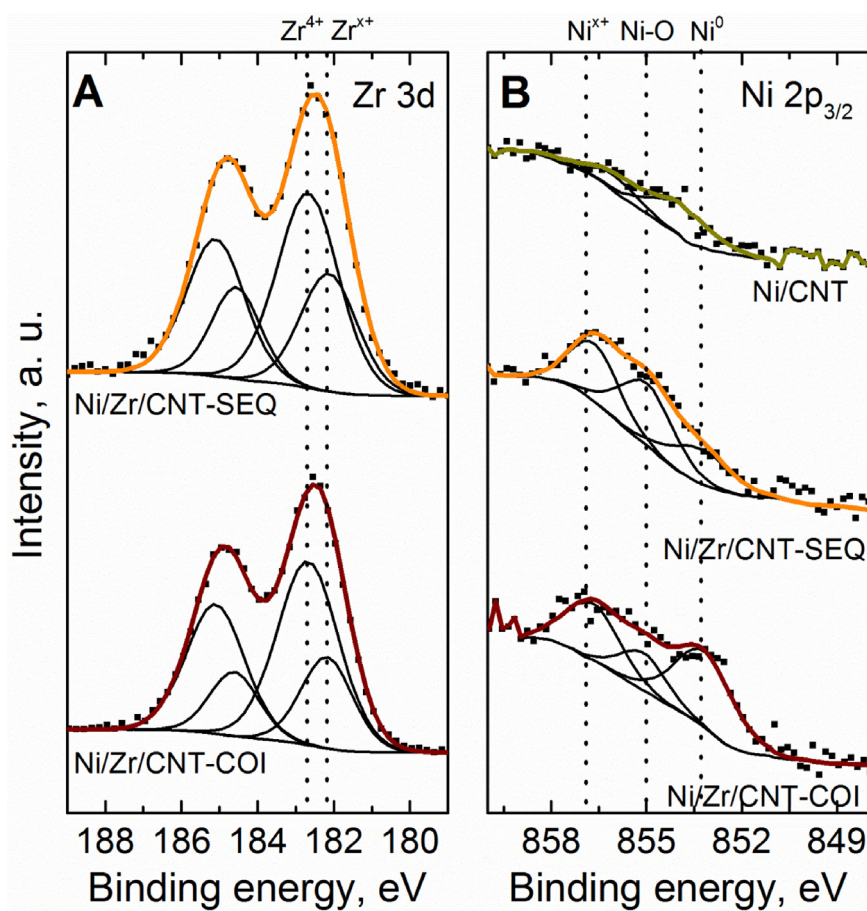


Fig. 3. XPS spectra and deconvoluted subbands of the different catalysts. Zr 3d band (A) and Ni 2p region (B).

temperature was necessary for hydrogen to reach the nickel surface. Additionally, H₂-TPR analyses have proven the CNTs did not suffer methanation below 500 °C, and that they were stable under the reaction conditions.

Fig. 3 displays Ni 2p_{3/2} and Zr 3d XPS spectra obtained for CNT supported catalyst. Fig. 3A shows that in both cases, Ni/Zr/CNT-SEQ and Ni/Zr/CNT-COI catalysts, the Zr 3d band can be fitted using two doublets: the one at higher binding energy (182.6 and 185.1 eV) is related to the formation of ZrO₂, and the one at lower binding energy (182.1 and 184.6 eV), in good agreement with the binding energy obtained when an alloy Zr–Ni with low Zr content is oxidized [29]. The binding energy of this new contribution (Zr^{x+}) is between the binding energy of Zr⁴⁺ and Zr³⁺, which are shift 1.06 eV [30]. Zr^{x+} corresponds with a new chemical state in which Zr–O bonds are more covalent than in the case of ZrO₂.

Ni 2p_{3/2} showed three different components (Fig. 3B). The first one, at 853.2 eV, is associated to metallic nickel (Ni⁰). This is the main contribution in the Ni/CNT sample. This binding energy is higher than the one expected for bulk Ni (852.7 eV). The same shift was observed by S. Zafeiratos et al. [31] for a 0.5 monolayer (ML) of Ni deposited onto ZrO₂. The higher binding energies values are due to initial and final effects resulting from the low coordination of Ni atoms in very small clusters or island. The other two components are centered at 855.0 and 856.6 eV, respectively. The signal at 855.0 eV corresponds to the oxidation of low coverage of Ni onto ZrO₂, as it has been reported [31], while the signal at 856.6 eV (Ni^{x+}) appears at a higher binding energy than the expected for nickel oxides (NiO at 854.6 eV and Ni₂O₃ at 856.1 eV).

For the sample Ni/CNT, without Zr, there is a contribution in the C 1s region at 283 eV related to the formation of Ni carbide (see

supplementary material). This contribution is not present in the other cases, and it further confirms that the new contribution corresponds with a new chemical state with Ni–O bonds more ionic than the ones of nickel oxides [32].

Summarizing, the Zr 3d has two components; one associated to ZrO₂ at 182.6 eV, and Zr^{x+}, which is at a lower binding energy. The Ni 2p_{3/2} binding energy for the highest oxidation state, Ni^{x+}, is also above that of nickel oxides. In the new chemical states, Ni–O bonds are more ionic and Zr–O bonds are more covalent than in pure Ni₂O₃ and ZrO₂ oxides. According to Barr [33] this behavior can be interpreted as due to the formation of a Zr–O–Ni mixed oxide, as has been observed in other systems as MgSeO₄, PbSiO₃, NiSiO₃ or Ti–O–Si [33,34]. In this work, the formation of this mixed oxide was only observed in catalysts with Zr in its composition, and presented the same contribution (~34% of total Ni) regardless of the method of preparation used (Table 1).

Fig. 4 shows the CO₂ desorption profiles of the samples. It could be observed that CNT showed only a very weak signal starting at 570 °C. This signal is likely to correspond to the CO₂ produced by CNT decomposition and not by the evolution of previously adsorbed CO₂. This is consistent with the thermogravimetric analysis of the CNTs under a flow of helium (see supplementary material), that show the CNTs only started to decompose at 575 °C. The CO₂ desorption profiles of Ni/Zr/CNT-SEQ and Ni/Zr/CNT-COI samples were similar, where three different signals can be clearly observed. This peaks have been proposed to represent three types of basic sites, a weak (α peak), moderate (β peaks), and strong (γ peak) basic sites, respectively. The most intense signal, centered about 100–150 °C, is ascribed to weakly basic sites related to the OH[–] groups of zirconia surface. On the other hand, moderate basic sites that appeared in the range 150–320 °C have been assigned to metal–oxygen pairs (Zr–O) [35]. Usually, this latter signal

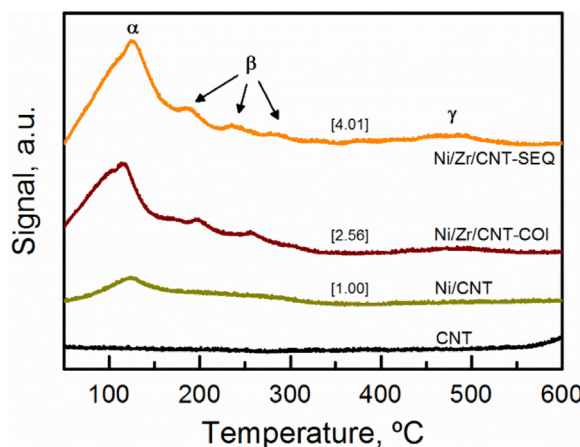


Fig. 4. CO_2 -TPD patterns of the CNT supported catalysts. The relative desorbed CO_2 (data in the bracket) was defined as the total amount of desorbed CO_2 per gram of catalyst with respect to that of Ni/CNT sample in the range 50–600 °C.

due to Zr–O shows only one kind of contribution [36]. However, in this work several types of contributions to moderate basic sites appeared, probably because the different interaction between ZrO_2 nanoparticles and CNT. Finally, centered about 490 °C appeared a low intensity signal due to strong basic sites, which were associated with low-coordination surface oxygen atoms [37,38]. On the other hand, Ni/CNT showed only a low signal in the weakly basicity zone which was extended slightly to the zone of moderate basicity. The relative amount of desorbed CO_2 , defined as the total amount of desorbed CO_2 per gram of catalyst with respect to that of the Ni/CNT sample in the range 50–600 °C, is showed within brackets in Fig. 4. These values indicated that the amount of CO_2 adsorbed by the zirconia-containing catalysts was considerable higher than for Ni/CNT sample. It must be also noted that the Ni/Zr/CNT-SEQ sample showed a notably greater CO_2 adsorption capacity than Ni/Zr/CNT-COI, even though both samples have the same composition. As suggested also by the TPR results, the catalyst impregnation method clearly affects the distribution and interaction of Ni and ZrO_2 , ultimately affecting the catalytic performance of each sample, as it will be confirmed next.

3.2. Activity and selectivity of Ni-catalyst in CO_2 methanation

Catalytic activity of the samples in CO_2 methanation was studied by monitoring the conversion of CO_2 as a function of temperature. The ignition or light-off curves between 200 and 500 °C, which are characterized by the temperatures at which 10 (T_{10}) and 50% (T_{50}) conversion was reached, are shown in Fig. 5A. The curve corresponding to the reaction over the pure CNT support confirmed no CO_2 conversion at all evaluated temperatures, confirming that all the activity results presented correspond exclusively to the CO_2 hydrogenation, with no measurable CNT decomposition and methanation. Furthermore, it can also be observed that the activity of the catalysts depended on the composition and the preparation method. Ni/Zr/CNT-SEQ catalyst showed the highest CO_2 conversion, with T_{10} and T_{50} values of 254 and 369 °C respectively. The CO_2 conversion increased with temperature, reaching a maximum value at about 400 °C. Further increase in reaction temperature resulted in decreased CO_2 conversion, due to the thermodynamic equilibrium of the exothermic CO_2 methanation, which favours the water reforming of methane (reverse Sabatier reaction). Additionally, the higher temperatures promote the reverse water gas shift reaction, increasing the CO production, thus reducing the CH_4 selectivity. For Ni/Zr/CNT-COI the observed activity was notably lower ($T_{10} = 310$ °C and $T_{50} \sim 500$ °C). Meanwhile, Ni/CNT catalyst presented an intermediate activity to those shown by the Zr-containing catalysts. Comparing activity of Ni/Zr/CNT-SEQ sample with other

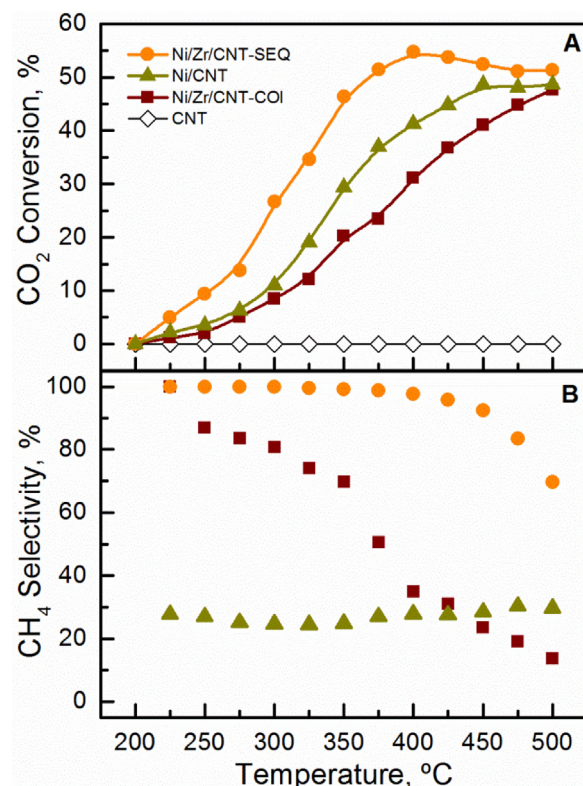


Fig. 5. A) CO_2 conversion light-off curves over different NiO-ZrO₂-CNT catalysts and CNT. B) Selectivity to CH_4 at different reaction temperatures of different catalysts.

studies that use similar reaction conditions, it can be observed that the values are very similar (within $\pm 5\%$ conversion values), even though in some of these work ceria-zirconia mix oxides are used as support [39–41].

During the CO_2 methanation reaction (1), the most likely byproduct is CO, originated by a partial reduction of CO_2 through the reverse WGS reaction (2).



Therefore, to entirely assess the catalytic performance, the selectivity to CH_4 must be evaluated for each catalyst (Fig. 5B). For the Ni/CNT sample the CH_4 selectivity is limited to only about 25–30% at all test temperatures. Meanwhile, Ni/Zr/CNT-COI catalyst shows a decreasing CH_4 selectivity from 100% at 225 °C, falling almost linearly to 16% at 500 °C. Finally, Ni/Zr/CNT-SEQ sample presents a completely different selectivity, as in this case the CH_4 selectivity was almost 100% up to 450 °C, and then decreased to 79% at 500 °C, because the conversion to CH_4 is limited by the reaction thermodynamics at high temperatures [42]. CH_4 production profile of this catalyst was equal to, or even higher, than observed in other CO_2 methanation studies with conventional Ni/ZrO₂ catalytic systems [43,44]. These results clearly confirm that, not only the catalytic activity, but also the selectivity to CH_4 and CO depended both on the composition as well as on preparation method.

Along with the light-off studies, catalyst stability was also tested for the best sample, subjecting the Ni/Zr/CNT-SEQ catalyst to long on-stream periods at reaction conditions (75.000 ml $\text{h}^{-1} \text{g}^{-1}$, 350 °C, 50 h). As shown in Fig. 6, CO_2 conversion remains constant during 50 h over this catalyst, with no important deactivation, indicating that the catalyst surface did not suffer major changes under reaction conditions. Additionally, the selectivity to CH_4 also remained constant with TOS,

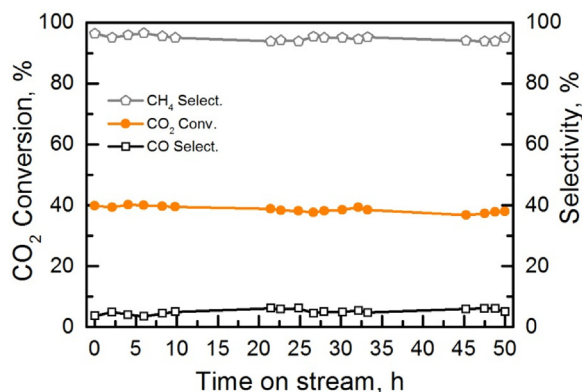


Fig. 6. CO₂ conversion vs. time on stream over Ni/Zr/CNT–COI catalyst (350 °C, 75.000 ml h⁻¹ g⁻¹).

with values around 95%.

The characterization and catalytic activity results presented so far clearly confirm an important effect of the preparation method on the catalytic performance of the samples supported on CNT, and that these differences will be determined by the physical configuration and interaction between the active phases. For this reason, the samples were analyzed by TEM in order to visualize if the arrangement of the various components were as different as to have such an important effect on the activity and selectivity.

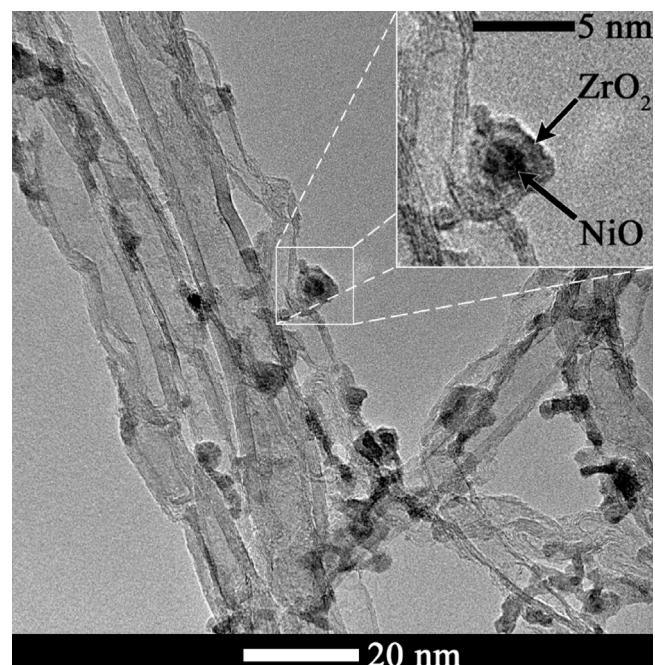


Fig. 8. TEM image of Ni/Zr/CNT-COI catalyst. Inset corresponds to a zoom of a NiO/ZrO₂ nanoparticle.

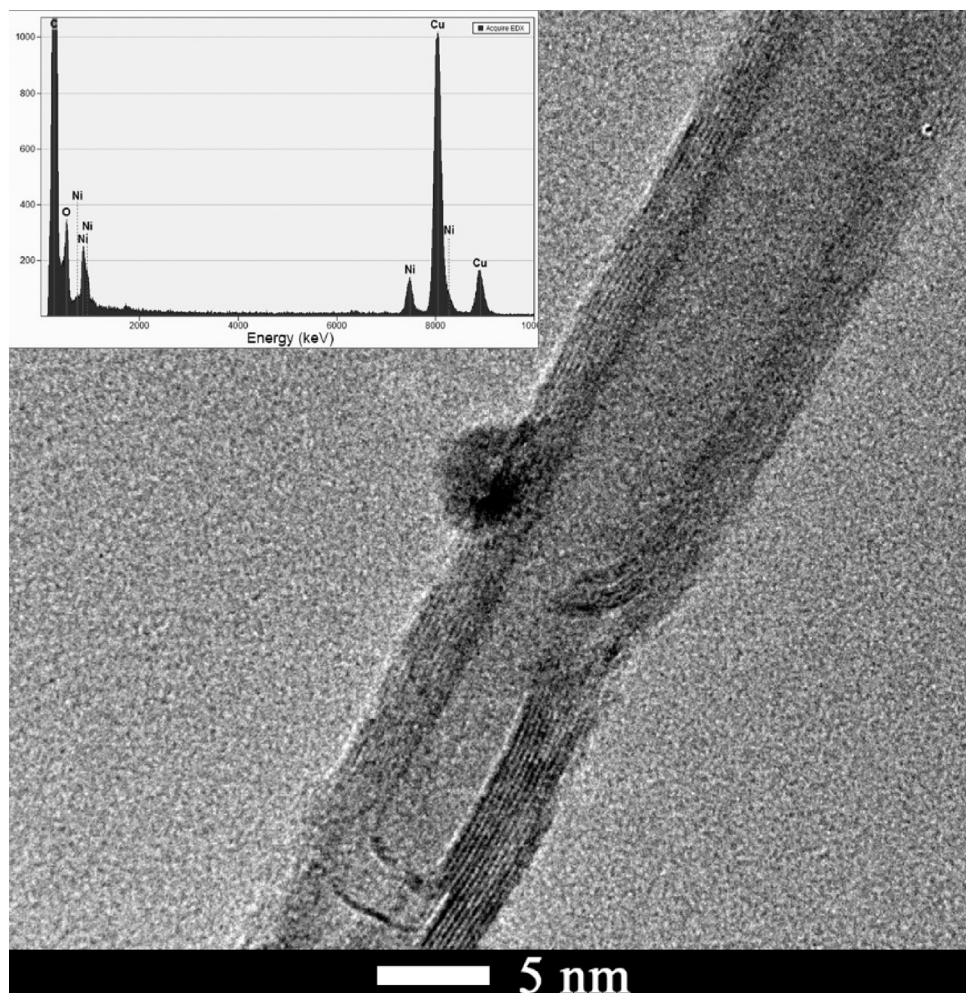


Fig. 7. TEM image of Ni/CNT sample. Inset: EDS spectrum of CNT and NiO nanoparticles. Copper peaks correspond to the grid used as support for the analysis.

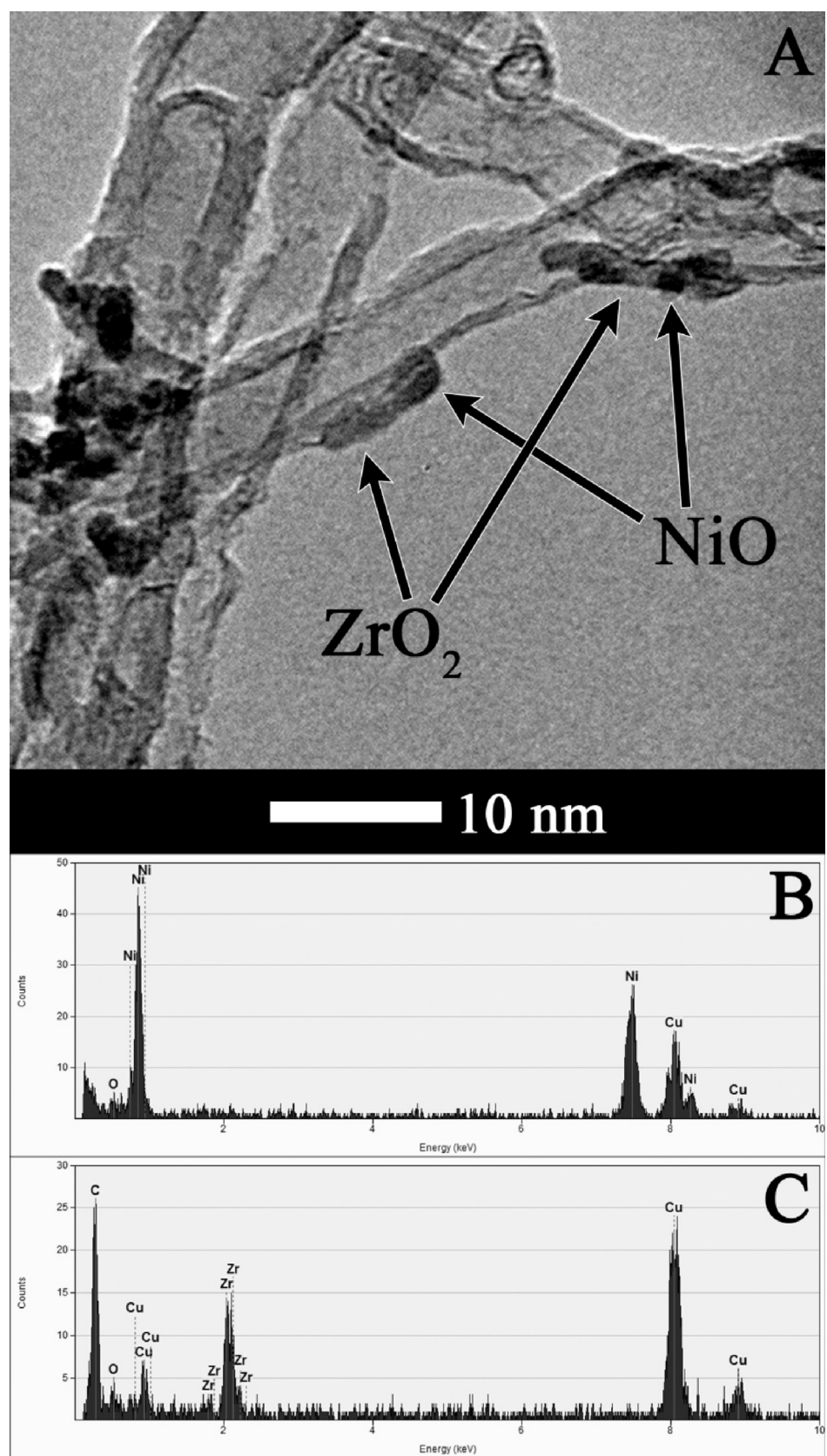


Fig. 9. TEM image of Ni/Zr/CNT-SEQ catalyst showing NiO and ZrO₂ nanoparticles (A). EDS spectra of a NiO nanoparticle (B). EDS spectra of a ZrO₂ nanoparticle (C).

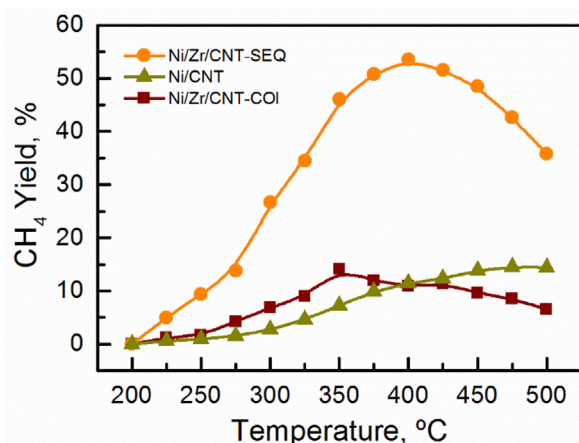


Fig. 10. CH_4 yield over different NiO-ZrO_2 -CNT catalysts at different reaction temperatures.

3.3. TEM analysis of Ni-catalyst

TEM analysis of the Ni/CNT sample exhibited CNT with NiO nanoparticles in order of 5 nm sizes (Fig. 7), which tend to grow only on the surface of the CNT as the parent CNT display their cup-ends close and, hence, the presence of Ni particles inside the tubes can be disregarded. Inset Fig. 7 corresponds to the linear EDS spectrum of CNT and NiO nanoparticles that confirms no contamination on the samples.

Fig. 8 corresponds to a representative TEM image of the sample Ni/Zr/CNT-COI. As it was suggested by the H_2 -TPR analysis, this micrograph confirms that the NiO nanoparticles are not directly exposed to the reactant atmosphere, as they are surrounded by ZrO_2 in a core-shell structure growing over the CNT (see inset in Fig. 8). Punctual EDS measurements performed by Scanning TEM (STEM) showed that the nucleus of these particles are NiO nanoparticles of nearly 4 nm, that were covered during the co-impregnation process by a ZrO_2 shell.

On the other hand, TEM analysis of Ni/Zr/CNT-SEQ sample (Fig. 9A) revealed that the initial impregnation of Zr precursor produces ZrO_2 elongated nanoparticles on the surface of the CNT, whose sizes range between 5 and 10 nm. The NiO nanoparticles deposited on a further step, can be found either on the surface or close to the ZrO_2 nanoparticles. Punctual EDS analyses performed in STEM mode to the different nanoparticles demonstrate the nearly pure composition of both types of nanoparticles, as it can be seen in Fig. 9B and C. It is clear then that, in the most active and selective sample, the NiO particles were available and exposed on the catalyst surface, and mostly in full contact with ZrO_2 .

3.4. Discussion

The characterization and activity results of Ni-ZrO_2 -CNT catalysts during CO_2 methanation presented in this work allow us to establish an important influence of the impregnation method on the catalytic performance of these systems, and provide insight of the reaction mechanism.

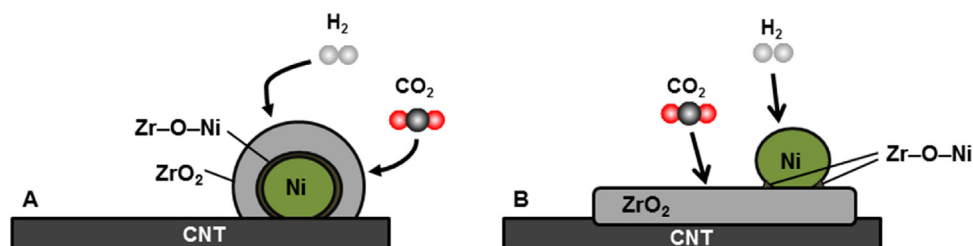


Fig. 11. Schematic representation of the disposition of NiO , ZrO_2 and interface Ni-O-Zr in the surface of CNT for Ni-Zr-CNT-COI (A) and Ni-Zr-CNT-SEQ catalysts (B).

In order to observe more clearly the catalytic behavior of the different catalysts in the whole range of temperatures tested, the CH_4 yield of each sample was calculated according to (3):

$$\text{Yield of } \text{CH}_4, \% = \frac{C_{\text{out}(\text{CH}_4)}}{C_{\text{in}(\text{CO}_2)}} \times 100 \quad (3)$$

The results obtained (Fig. 10) showed that the Ni/CNT and Ni/Zr/CNT-COI catalysts showed a similar CH_4 yield, with values lower than 15% at all tested temperatures. In contrast, the values observed for the Ni/Zr/CNT-SEQ catalyst were significantly higher than in the other cases, indicating a better catalytic behavior of this sample.

H_2 -TPR and CO_2 -TPD results suggest that Ni is partially blocked in the Ni/Zr/CNT-COI catalyst affecting its catalytic performance. On the contrary, a higher proportion of Ni-O species exposed to the gas phase (evidenced by XPS results (Table 1)) in Ni/Zr/CNT-SEQ catalyst favored its best catalytic behavior in CO_2 methanation. Furthermore, the formation of Zr-O-Ni mixed oxide confirms the results observed in the H_2 -TPR analysis, showing a close interaction between Ni and Zr.

TEM analyses of the three catalysts were also in agreement with the characterization exposed above. On the one hand, H_2 -TPR analyses showed a similar reduction profiles for Ni/CNT and Ni/Zr/CNT-SEQ samples, indicating a similar dispersion and availability of NiO nanoparticles on the surface of these catalysts. This fact was verified by TEM analysis of both samples, where it was observed a similar size and dispersion of NiO nanoparticles and any covering/block of these nanoparticles by the zirconia in the catalyst Ni/Zr/CNT-SEQ. On the other hand, CO_2 -TPD analyses showed similar profiles for the catalysts with ZrO_2 in its composition, and a greater CO_2 adsorption for the catalyst prepared by sequential impregnation. This was also in accordance with evinced by the TEM of these two samples, as in Ni/Zr/CNT-SEQ catalyst almost all zirconia is dispersed and available on the surface of CNTs, while in the case of the Ni/Zr/CNT-COI catalyst, a great proportion of zirconia is surrounding the NiO nanoparticles and showed greater agglomeration.

This explains the lower catalytic activity of the Ni/Zr/CNT-COI catalyst, since the zirconia was blocking the access to most of the NiO nanoparticles. In addition, the ZrO_2 is not able to dissociate H_2 , and it could only activate CO_2 molecules to CO [40]. This fact was confirmed with selectivity results obtained with this catalyst (Fig. 5B), which indicated low and decreasing CO_2 conversion to CH_4 .

Then, CO_2 molecules were activated on the ZrO_2 surface favored by its oxygen vacancies or basic sites observed by CO_2 -TPD [45], while dihydrogen molecules were dissociated on the Ni surface [43]. Therefore, by increasing the extent of the Ni – ZrO_2 interface, the interaction between hydrogen atoms and activated CO_2 molecule can be facilitated, increasing the reaction rate and selectivity towards CH_4 . The Ni – ZrO_2 interface is indicated by the formation of a Zr-O-Ni mixed oxide, as was observed by XPS. As can be seen in Table 1, the presence of the mixed oxide was very similar in both catalysts, since the abundance of Ni^{x+} and Zr^{x+} was similar in both samples. The difference was that in the case of the Ni/Zr/CNT-SEQ catalyst the Ni – ZrO_2 interface was accessible to the reaction gases, favoring the combination of hydrogen atoms and activated CO_2 . In contrast, in the case of Ni/Zr/CNT-COI, the interface is inside the ZrO_2 shell, and is inaccessible to the reagents

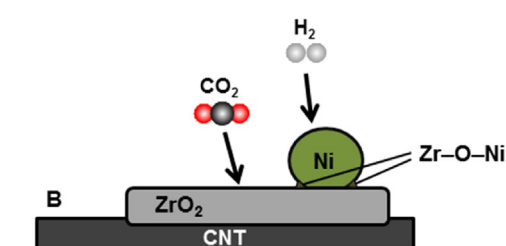


(Fig. 11). This was the reason why the Ni/Zr/CNT-SEQ catalyst was the most active in CO₂ methanation and presented the highest selectivity to CH₄ at all tested temperatures. In contrast, Ni/CNT sample showed lower activity than Ni/Zr/CNT-SEQ catalyst, despite having all the nickel on the surface of the CNT. In this case, Ni nanoparticles should activate the CO₂ and dissociate the H₂, since CNT are inert to both processes. Although Ni/CNT catalyst has no ZrO₂ present on its structure, the CO₂-TPD analysis (Fig. 7) have shown that the NiO/Ni nanoparticles were able to fix a small amount of CO₂. This fact along with the ability of the Ni nanoparticles to dissociate H₂, made the activity of this catalyst greater than that of Ni/Zr/CNT-COI, where most of the NiO nanoparticles is covered by ZrO₂ shell.

4. Conclusions

CNT supported Nickel-ZrO₂ catalysts were prepared by sequential impregnation and co-impregnation in order to obtain catalysts with different distribution and interaction of active species. In order to correlate these properties to the catalytic performance during CO₂ methanation, the catalysts were characterized by XRD, TGA, H₂-TPR, CO₂-TPD, TEM and XPS techniques.

The synthesized samples exhibited high activity, though the sample which showed best results was prepared by sequential impregnation, as it displayed the maximum activity and the better selectivity to CH₄. Additionally, this catalyst showed very notable stability during long time on stream, since its activity and selectivity remained constant after 50 h of reaction. The characterization of the catalysts showed important differences in their properties and in the disposition of active phases in CNT surface in function of the impregnation method used. H₂-TPR showed a greater reduction capacity at lower temperatures for the Ni/Zr/CNT-SEQ catalyst, showing a similar reduction profile as Ni/CNT sample. Meanwhile, CO₂-TPD analyses showed a similar basicity profile for Ni/Zr/CNT-COI and Ni/Zr/CNT-SEQ samples, although the sample prepared by sequential impregnation presented a 1.5 times greater basicity. TEM analyses confirmed that in Ni/Zr/CNT-SEQ catalyst NiO nanoparticles are available and deposited either on the surface or next to ZrO₂ nanoparticles. However, the catalyst prepared by co-impregnation showed that NiO nanoparticles were surrounded by ZrO₂ in a core-shell structures that growth over the CNT, preventing access to Ni and to Ni – ZrO₂ interface. This arrangement of Ni and ZrO₂ on the surface of the CNT was responsible for the better catalytic performance shown by the catalyst prepared by sequential impregnation. In this case, by increasing the proportion of these Ni–O–Zr exposed species, the interaction between hydrogen atoms, dissociated on Ni surface, and CO₂ molecule, activated by ZrO₂, can be facilitated, increasing then the reaction rate and selectivity towards CH₄.

Acknowledgements

Financial support from CONICYT-Chile is gratefully acknowledged: Project PAI 79170079 (N.B.). Project PIA/APOYO CCTE AFB170007 (N.E.). Project FONDECYT Regular 1171193 (F.G.). Authors F.G. and R.E. acknowledge the support of MINECON-Chile through project Millennium Nucleus MULTIMAT - ICM/MINECON.

References

- [1] S. Rönsch, J. Schneider, S. Matthischke, M. Schlüter, M. Götz, J. Lefebvre, P. Prabhakaran, S. Bajohr, *Fuel* 166 (2016) 276–296.
- [2] P. Sabatier, J.B. Senderens, *New synthesis of methane, Compt. Rend.* 134 (1902) 514–516.
- [3] G. Garbarino, D. Bellotti, E. Finocchio, L. Magistri, G. Busca, *Catal. Today* 277 (2016) 21–28.
- [4] C. Janke, M.S. Duyar, M. Hoskins, R. Farrauto, *Appl. Catal. B: Environ.* 152–153 (2014) 184–191.
- [5] A. Karelovic, P. Ruiz, *J. Catal.* 301 (2013) 141–153.
- [6] J.-N. Park, E.W. McFarland, *J. Catal.* 266 (2009) 92–97.
- [7] I. Grac, L.V. González, M.C. Bacariza, A. Fernandes, C. Henriques, J.M. Lopes, M.F. Ribeiro, *Appl. Catal. B: Environ.* 147 (2014) 101–110.
- [8] R.V. Goncalves, L.L.R. Vono, R. Wojcieszak, C.S.B. Dias, H. Wender, E. Teixeira-Neto, L.M. Rossi, *Appl. Catal. B: Environ.* 209 (2017) 240–246.
- [9] S. Rahmani, M. Rezaei, F. Meshkani, *J. Ind. Eng. Chem.* 20 (2014) 1346–1352.
- [10] Y. He, M.E. Ford, M. Zhu, Q. Liu, U. Tumuluri, Z. Wu, I.E. Wachs, *Appl. Catal. B: Environ.* 193 (2016) 141–150.
- [11] P.M. More, D.L. Nguyen, M.K. Dongare, S.B. Umbarkar, N. Nuns, J.-S. Girardon, C. Dujardin, C. Lancelot, A.-S. Mamede, P. Granger, *Appl. Catal. B: Environ.* 162 (2015) 11–20.
- [12] A.B. Dongil, I.T. Ghompson, R. García, J.L.G. Fierro, N. Escalona, *RSC Adv.* 6 (2016) 2611–2623.
- [13] L. Jaramillo Zapata, E. Moncada Acevedo, *Environmental applications of nanomaterials: new technologies for sustainable development*, in: Z. Bartul, J. Trenor (Eds.), *Advances in Nanotechnology*. vol. 12, Nova Science Publishers, New York, 2014, pp. 221–264.
- [14] N.I. Andersen, A. Serov, P. Atanassov, *Appl. Catal. B: Environ.* 163 (2015) 623–627.
- [15] W. Wang, W. Chu, N. Wang, W. Yang, C. Jiang, *Int. J. Hydrogen Energy* 41 (2016) 967–975.
- [16] L. Liu, H. Lou, M. Chen, *Int. J. Hydrogen Energy* 41 (2016) 14721–14731.
- [17] A.B. Dongil, L. Pastor-Perez, N. Escalona, A. Septúlveda-Escribano, *Carbon* 101 (2016) 296–304.
- [18] L. Chen, Y. Bao, Y. Sun, D. Ma, D. Yea, B. Huang, *Catal. Sci. Technol.* 6 (2016) 98–106.
- [19] S. Brunauer, P.H. Emmett, E. Teller, *J. Am. Chem. Soc.* 60 (1938) 309–319.
- [20] M. Mohammadi, B. Khoshnevisan, Sh. Varshoy, *Int. J. Hydrogen Energy* 41 (2016) 10311–10315.
- [21] Z. Tian, C. Liu, Q. Li, J. Hou, Y. Li, S. Ai, *Appl. Catal. A: Gen.* 506 (2015) 134–142.
- [22] E.R. Shaaban, M.A. Kaid, M.G.S. Ali, *J. Alloys Compd.* 613 (2014) 324–329.
- [23] A. Qurashi, Z. Zhang, M. Asif, T. Yamazaki, *Int. J. Hydrogen Energy* 40 (2015) 15801–15805.
- [24] V.G. Deshmane, Y.G. Adewuyi, *Microporous Mesoporous Mater.* 148 (2012) 88–100.
- [25] S.K. Gupta, D. Chandrasekhar, R.M. Kadam, *J. Mol. Struct.* 1102 (2015) 141–145.
- [26] H.J. Huang, M.C. Wang, *Ceram. Int.* 39 (2013) 1729–1739.
- [27] D. Ping, C. Wang, X. Dong, Y. Dong, *Appl. Surf. Sci.* 369 (2016) 299–307.
- [28] X. Yang, X. Wang, G. Gao, Wendumira, E. Liu, Q. Shi, J. Zhang, C. Han, J. Wang, H. Lu, J. Liu, M. Tong, *Int. J. Hydrogen Energy* 38 (2013) 13926–13937.
- [29] B. Walz, P. Oelhafen, H.-J. Güntherodt, A. Baiker, *Appl. Surf. Sci.* 37 (1989) 337–352.
- [30] C. Morant, J.M. Sanz, L. Galán, L. Soriano, F. Rueda, *Surf. Sci.* 218 (1989) 331–345.
- [31] S. Zafeiratos, S. Kennou, *Surf. Sci.* 266 (2001) 482–485.
- [32] I. Czekaj, F. Loviat, F. Raimondi, J. Wambach, S. Biollaz, A. Wokaun, *Appl. Catal. A: Gen.* 329 (2007) 68–78.
- [33] T.L. Barr, *J. Vac. Sci. Technol. A* 9 (1991) 1793–1805.
- [34] N. Benito, C. Palacio, *J. Phys. D: Appl. Phys.* 47 (2014) 0153087pp.
- [35] X. Dong, F. Li, N. Zhao, F. Xiao, J. Wang, Y. Tan, *Appl. Catal. B: Environ.* 191 (2016) 8–17.
- [36] P. Gao, F. Li, H. Zhan, N. Zhao, F. Xiao, W. Wei, L. Zhong, H. Wang, Y. Sun, *J. Catal.* 298 (2013) 51–60.
- [37] G. Wu, X. Wang, W. Wei, Y. Sun, *Appl. Catal. A: Gen.* 377 (2010) 107–113.
- [38] D. Wierzbicki, R. Debek, M. Motak, T. Grzybek, M.E. Gálvez, P. Da Costa, *Catal. Commun.* 83 (2016) 5–8.
- [39] P.A. Ussa Aldana, F. Ocampo, K. Kobl, B. Louis, F. Thibault-Starzyk, M. Daturi, P. Bazin, S. Thomas, A.C. Roger, *Catal. Today* 215 (2013) 201–207.
- [40] Q. Pan, J. Peng, T. Sun, S. Wang, S. Wang, *Catal. Commun.* 45 (2014) 74–78.
- [41] H. Takano, Y. Kirihata, K. Izumiya, N. Kumagai, H. Habazaki, K. Hashimoto, *Appl. Surf. Sci.* 388 (2016) 653–663.
- [42] R.Y. Chein, W.Y. Chen, C.T. Yu, *J. Nat. Gas Sci. Eng.* 29 (2016) 243–251.
- [43] F. Ocampo, B. Louis, L. Kiwi-Minsker, A.-C. Roger, *Appl. Catal. A: Gen.* 392 (2011) 36–44.
- [44] J. Ren, X. Qin, J.-Z. Yang, Z.-F. Qin, H.-L. Guo, J.-Y. Lin, Z. Li, *Fuel Process. Technol.* 137 (2015) 204–211.
- [45] G. Garbarino, P. Riani, L. Magistri, G. Busca, *Int. J. Hydrogen Energy* 39 (2014) 11557–11565.

[1] S. Rönsch, J. Schneider, S. Matthischke, M. Schlüter, M. Götz, J. Lefebvre,